Inorganic Chemistry

Article

pubs.acs.org/IC

Water Oxidation Catalysis: Influence of Anionic Ligands upon the Redox Properties and Catalytic Performance of Mononuclear Ruthenium Complexes

Lianpeng Tong,[†] Ying Wang,[‡] Lele Duan,[†] Yunhua Xu,[†] Xiao Cheng,[‡] Andreas Fischer,[†] Mårten S. G. Ahlquist,*[,‡] and Licheng Sun*[,†,§]

[†]Department of Chemistry, School of Chemical Science and Engineering, and [‡]Department of Theoretical Chemistry & Biology, School of Biotechnology, KTH Royal Institute of Technology, 100 44 Stockholm, Sweden

[§]State Key Laboratory of Fine Chemicals, DUT−KTH Joint Education and Research Center on Molecular Devices, Dalian University of Technology (DUT), 116024 Dalian, China

Supporting Information

ABSTRACT: Aiming at highly efficient molecular catalysts for water oxidation, a mononuclear ruthenium complex $Ru^{II}(hqc)(pic)_3$ (**1**; H_2hqc = 8-hydroxyquinoline-2-carboxylic acid and pic = 4-picoline) containing negatively charged carboxylate and phenolate donor groups has been designed and synthesized. As a comparison, two reference complexes, $Ru^{II}(pdc)(pic)_3$ (**2**; H_2pdc = 2,6-pyridine-dicarboxylic acid) and $Ru^{II}(tpy)(pic)_3$ (**3**; tpy = 2,2′:6′,2″-terpyridine), have also been prepared. All three complexes are fully characterized by NMR, mass spectrometry (MS), and X-ray crystallography. Complex **1** showed a high efficiency toward catalytic water oxidation either driven by chemical oxidant (Ce^{IV} in a pH 1 solution) with a initial turnover number of 0.32 s^{-1}, which is several orders of magnitude higher than that of related mononuclear ruthenium catalysts reported in the literature, or driven by visible light in a three-component system with $[Ru(bpy)_3]^{2+}$ types of photosensitizers. Electrospray ionization MS results revealed that at the Ru^{III} state complex **1** undergoes ligand exchange of 4-picoline with water, forming the authentic water oxidation catalyst in situ. Density functional theory (DFT) was employed to explain how anionic ligands (hqc and pdc) facilitate the 4-picoline dissociation compared with a neutral ligand (tpy). Electrochemical measurements show that complex **1** has a much lower $E(Ru^{III}/Ru^{II})$ than that of reference complex **2** because of the introduction of a phenolate ligand. DFT was further used to study the influence of anionic ligands upon the redox properties of mononuclear aquaruthenium species, which are postulated to be involved in the catalysis cycle of water oxidation.

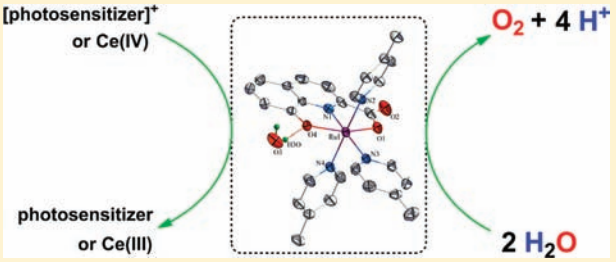

INTRODUCTION

Through a delicate photosynthetic system, green plants, algae, and cyanobacteria can capture sunlight and directly convert it into energy-rich compounds by reduction of CO_2 at one side and oxidation of water at the other side.[1] The development of an artificial photosynthesis (AP) system that can mimic solar-energy conversion in nature is, however, held back by the lack of qualified water oxidation catalysts (WOCs) for the O_2-evolving reaction $2H_2O \rightarrow O_2 + 4H^+ + 4e^-$.[2]

One of the key requirements of a qualified WOC is that it shows high efficiency, generally meaning high turnover frequency (TOF). Only with high enough catalytic activity could WOCs seize electrons from water molecules effectively and meanwhile avoid charge accumulation or electron recombination in an integrated photosensitizer (PS)−catalyst molecule assembly toward AP.[3] Moreover, WOCs have to possess low catalytic overpotential so as to be matched with the oxidation potential of PSs.[4] These two features of WOCs, high efficiency and low overpotential, are also most desired from the perspective of electrochemical water splitting in practice[5] (electrolysis of water splitting can be regarded as a certain kind of AP system, where the power of electrolysis is generated from solar energy[6]).

The difficulty of the design and preparation of applicable WOCs lies primarily in the complexity of the water oxidation/O_2-evolving reaction, which involves the removal of four electrons and four protons from two water molecules and the formation of an O−O bond, besides the harsh thermodynamic demand (E^0 = 1.23 V vs NHE at pH 0).[7] Since the discovery of well-known "blue dimer" $[(bpy)_2Ru(H_2O)(\mu\text{-}O)(H_2O)Ru(bpy)_2]^{4+}$ (bpy = 2,2′-bipyridine) by Meyer et al. in the early 1980s,[8] ruthenium complexes have been regarded as potential candidates to mimic the oxygen-evolving center (OEC) in green plants. Because of their versatile redox properties, aquaruthenium complexes can access high oxidation states and form Ru-oxo species across a narrow potential gap by a proton-coupled electron-transfer (PCET) pathway.[9] It had been initially assumed,

Received: July 1, 2011
Published: February 24, 2012

   dx.doi.org/10.1021/ic201348u | *Inorg. Chem.* 2012, 51, 3388−3398

Scheme 1. Molecular Formulas of 1−3

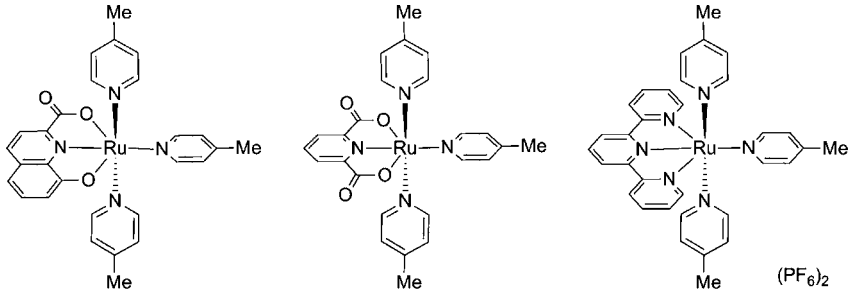

$Ru^{II}(hqc)(pic)_3$ (**1**) (this work)

$Ru^{II}(pdc)(pic)_3$ (**2**) (by our group)[14]

$Ru^{II}(tpy)(pic)_3$ (**3**) (by Thummel's group)[11a]

inspired by OEC and "blue dimer", that multiple metal cores were necessary to accomplish the water oxidation reaction. Then, in 2005, Zong and Thummel reported a suite of mononuclear aquaruthenium(II) complexes capable of driving water oxidation with moderate activity in the presence of a chemical oxidant: $Ce^{IV}(Ce(NH_4)_2(NO_3)_6)$.[10] Over the last several years, a number of examples of both mononuclear aqua- and non-aquaruthenium(II) complexes with a simple polypyridyl ligand have been reported to be active toward water oxidation.[11] Extensive investigation of mononuclear ruthenium(II) WOCs, from both experimental and theoretical aspects, has provided insight into the catalytic mechanism.[12] The discovery of these mononuclear ruthenium(II) WOCs is one of the major breakthroughs recently in the context of catalytic water oxidation and has drawn more and more attention: their simple structures allow straightforward preparation and modification, well-defined photo- and eletrospectroscopic properties, and efficient utilization of the noble metal.

Most of the studied mononuclear ruthenium(II) WOCs contain a ruthenium core coordinatively saturated with neutral N-donor ligands of different dentates; for example, $Ru^{II}(tpy)(pic)_3$ (complex **3** in Scheme 1; tpy = 2,2′:6′,2″-terpyridine and pic = 4-picoline), which was first studied as a WOC by Thummel's group, adapts a typical coordination matrix as a representative of such mononuclear ruthenium(II) WOCs.[11a] Our recent study illustrated that one picoline ligand of complex **3** could be slowly replaced by H_2O in an acidic cerium(IV) aqueous solution, forming a aquaruthenium(III) species as the active WOC.[13] A similar, but much faster, ligand-exchange process was also observed for $Ru^{II}(pdc)(pic)_3$ (complex **2** in Scheme 1; H_2pdc = 2,6-pyridinedicarboxylic acid) by our group.[14] Despite similar ligand motifs between **2** and **3**, the introduction of an anionic pdc ligand gives complex **2** a much higher catalytic activity (initial TOF = 0.23 s^{-1}) compared with that of complex **3** (TOF = 0.035 s^{-1}; there is a period of induction; see the details in ref 13). In fact, complex **2** is one of the most active ruthenium WOCs after the dinuclear ruthenium WOC reported recently.[15] Furthermore, complex **2** shows a low catalytic overpotential toward water oxidation and can be combined with $[Ru(bpy)_3]^{2+}$ types of PSs to achieve homogeneous visible-light-driven water oxidation at neutral pH. The strong influence of an anionic ligand (carboxylate) on ruthenium WOCs, we believe, could be very important in the context of AP, where an efficient WOC with a low overpotential is indispensable.

Aiming at further optimization of the ruthenium WOCs, we synthesized a novel mononuclear ruthenium(II) complex, $Ru^{II}(hqc)(pic)_3$ (complex **2** in Scheme 1; H_2hqc = 8-hydroxyquinoline-2-carboxylic acid), by replacing one of the coordinated carboxylate ligands of **2** with a phenolate group. The introduction of O-donor ligands leads to destabilization of the filled d orbitals of the low-valent ruthenium complexes, due to $d\pi-p\pi$ repulsion. At the same time, these anionic ligands (carboxylate and phenolate) can stabilize the higher oxidation states of ruthenium complexes by favorable interaction between the filled p orbitals of O atoms and empty d orbitals of the metal. We herein report the preparation, structure, electrochemical properties, and catalytic performance of complex **1**. **2** and **3** were also synthesized and examined as reference compounds in this work. A comparative investigation of complexes **1**−**3** by both experimental and theoretical studies is conducive to our understanding of how the coordination sphere of ruthenium(II) WOCs affects their chemical properties and catalytic activity.

EXPERIMENTAL SECTION

General Considerations. *cis*-$Ru(DMSO)_4Cl_2$,[16] $[Ru^{II}(tpy)(pic)_3](PF_6)_2$ (**3**),[11a] $Ru^{II}(bpy)_2(dcbpy)(PF_6)_2$ [**P2**; dcbpy = 4,4′-bis-(ethoxycarbonyl)-2,2′-bipyridine],[17] and $Ru^{II}(bpy)(dcbpy)_2(PF_6)_2$ (**P3**)[18] were prepared according to the literature methods. The synthesis of $Ru^{II}(pdc)(pic)_3$ (**2**) was reported in our previous work.[14] 8-Hydroxyquinoline-2-carboxylic acid, $[Ru^{II}(bpy)_3]Cl_2{\cdot}6H_2O$ (**P1**), $RuCl_3{\cdot}xH_2O$, sodium persulfate, and pH 7.0 phosphate buffer (50 mM) were purchased from Aldrich. All other reagents and solvents are commercially available and used as received, unless otherwise noted. Water used in syntheses and measurements was deionized by a Milli-Q technique. ^1H NMR spectra were recorded with a Bruker Advance 500 spectrometer. Mass spectrometry (MS) measurements were performed on a Finnigan LCQ Advantage MAX mass spectrometer. UV−vis spectra were obtained using a PerkinElmer Lambda 750 UV−vis spectrophotometer. Elemental analyses were performed with a Thermoquest-Flash EA 1112 apparatus. Diffraction data of crystal structures were collected on a Bruker-Nonius Kappa CCD using Mo Kα. Cyclic voltammetric (CV) measurements were carried out with an Autolab potentiostation and a GPES electrochemical interface (Eco Chemie) using a glassy carbon disk (diameter = 3 mm) as the working electrode and a platinum wire as the counter electrode. The reference electrode was Ag/Ag^+ (0.1 m $AgNO_3$ in acetonitrile) for a nonaqueous solution or Ag/AgCl (3 M KCl aqueous solution) for an aqueous solution. The electrolytes used were 0.1 M Bu_4NPF_6 in a corresponding organic solvent, an aqueous solution of CF_3SO_3H (pH 1.0) containing 10% acetonitrile, or pH 7.0 phosphate buffer (50 mM) containing 10% acetonitrile. Ferrocene (Fe^{III}/Fe^{II} = 0.63 V vs NHE) was used as an external reference in an organic medium and $Ru^{II}(bpy)_3Cl_2$ (Ru^{III}/Ru^{II} = 1.26 V vs NHE) in an aqueous medium.

Oxygen Evolution Measurement. The gas chromatograph employed for O_2 detection is an Agilent Technologies Series 3000A micro gas chromatograph equipped with a thermal conductivity detector and a 5 Å molecular sieve column (12 mm/320 mm/10 m) using helium as the carrying gas.

dx.doi.org/10.1021/ic201348u | Inorg. Chem. 2012, 51, 3388−3398

In a typical run of chemical-driven water oxidation using cerium(IV), a 25 mL round-bottomed flask was charged with 3 mL of a Ce^{IV}/CF_3SO_3H aqueous solution (pH 1.0; the concentration of Ce^{IV} is 0.083 M) and deaerated with helium until no obvious background oxygen was observed by gas chromatography (GC) in the system. Then, the catalyst (50 μL, 1 mM in acetonitrile) was injected into the homogeneous solution through a septum cap. The amount of evolved O_2 was monitored by an oxygen sensor (Ocean Optics FOXY-OR125-G probe and Ocean Optics MFPF-100 fluorimeter). Raw data from the sensor were collected by the Tau Theta Host Program and simultaneously converted into the percentage of O_2 by an OOIS application. At the end of a measurement, a gas sample was purged into the gas chromatograph for determination of the evolved O_2 amount. The initial rates of O_2 generation at different catalyst concentrations were measured with a pressure transducer (Omega PX138-030A5 V) driven at 8.00 V (power supply TTi-PL601) and a data acquisition module (Omega OMB-DAQ-2416; running at 2 Hz for our measurements).

In a typical run of visible-light-driven water oxidation, a 100 mL round-bottomed flask was charged with 10 mL of pH 7.2 phosphate buffer (20 mM), 0.55 mL of acetonitrile, catalyst (55.0 μM), PS (550 μM), and electron acceptor $Na_2S_2O_8$ (10 mM). The flask was maintained in a circulating water-cooling system and connected to the gas chromatograph via a $^1/_{16}$ in. gas sampling tube. After 30 min of deaeration with helium, the mixture was irradiated by a xenon lamp (500 W) with a $\lambda > 400$ nm filter (the intensity of irradiation was ~0.3 W cm^{-2}), and the generated O_2 was measured by GC every 5 min.

A Clark-type oxygen electrode (DW2/2 unit with an S1 electrode) was also applied to monitor light-driven water oxidation (more information about the Clark-type electrode can be obtained from the web site of Hansatech Instruments Ltd.).

Quantum Yield Measurement. A reaction vessel, charged with 20 mL pH 7.2 phosphate buffer (20 mM) and 1.1 mL of acetonitrile, catalyst **1** (55.0 μM), PS **P3** (550 μM), and electron acceptor $Na_2S_2O_8$ (10 mM), was thoroughly deaerated with helium before irradiation. The volume of evolved O_2, after 5 min of irradiation, was measured by GC and converted to the molar amount. The light source is a collimated Nichia 445 nm laser diode, and a Galilean beam expander was used to control the strength of irradiance. The incident radiant power was measured by a calibrated laser power meter (Ophir Optronics Nova II) and a thermopile sensor (Ophir Optronics 3A-P-FS).

Synthesis of $Ru^{II}(hqc)(pic)_3$ (1). An in situ solution of disodium 8-hydroxyquinoline-2-carboxylate (Na_2hqc) was prepared by dissolving 56.7 mg of H_2hqc (0.3 mmol) in 3 mL of a water/methanol (1:1) solution of NaOH (40 mg, 0.6 mmol). This Na_2hqc solution was then slowly dropped into a methanol solution (12 mL) of $Ru(DMSO)_4Cl_2$ (145.2 mg, 0.3 mmol). The mixture was degassed by N_2 and was heated to reflux under N_2. The color of this solution gradually became dark red from light yellow. After 12 h of reflux, an excess of 4-picoline (0.5 mL) was added and the mixture was kept refluxing for another 6 h. After cooling, the solvent of the reaction mixture was removed in a vacuum and the residues were washed with diethyl ether. The remaining oily part was dissolved in CH_2Cl_2 (15 mL) and washed with water (10 mL × 3) to remove organic salt. The organic layer was dried over $MgSO_4$, and the raw product was obtained by evaporation of the solvent. After purification by chromatography over silica with methanol/CH_2Cl_2 (3:97, v/v), complex **1** was afforded as a dark-red solid (80 mg, 47% yield). ^{1}H NMR (500 MHz, CD_2Cl_2): δ 8.77 (d, J = 5.0 Hz, 2H), 8.24 (d, J = 5.5 Hz, 4H), 7.60 (m, 2H), 7.29 (t, J = 7.5 Hz, 1H), 7.15 (d, J = 5.5 Hz, 2H), 6.89 (d, J = 5.5 Hz, 4H), 6.74 (m, 2 H), 2.40 (s, 3H), 2.22 (s, 6H). MS (ESI^+). Calcd: m/z 569.11 ($M + H^+$). Found: m/z 568.94. Calcd: m/z 591.09 ($M + Na^+$). Found: m/z 590.84. Elem anal. Calcd for $C_{28}H_{26}N_4O_3Ru{\cdot}1.5H_2O$: C, 56.56; H, 4.92; N, 9.42. Found: C, 56.06; H, 4.60; N, 9.30.

Theoretical Studies. All density functional theory (DFT) calculations were carried out with the *Jaguar 7.6* program package by Schrödinger LLC. For geometry optimizations, solvation energy, and frequency calculations, Becke's three-parameter hybrid functional and the LYP correlation functional (B3LYP)[19] were used with the LACVP** core potential and basis set, while single-point energy corrections were performed with the M06[20] functional using the LACV3P**++ basis set, which, as suggested by Martin,[21] was augmented with two f-polarization functions on ruthenium. Frequency calculations were performed on the optimized geometries to verify that the geometries correspond to minima or first-order saddle points (transition states) on the potential energy surface. The Gibbs free energies were defined as the following equation: $G = E$(M06/LACV3P**++2f on Ru) + G_{solv} + ZPE + H_{298} + TS_{298} + 1.9 [concentration correction to the free energy of solvation from M(g) → M(aq) to atm(g) → M(aq)]. The solvation model applied was the Poisson−Boltzmann reactive field implemented in *Jaguar 7.6*.[22] We have noticed that the pK_a values of acidic protons deviated by a few units; however, when explicit water molecules were included in hydrogen bonding with these protons, an excellent agreement with experiments was achieved. Hence, all aqua and hydroxy complexes include one explicit water per hydrogen on the aqua or hydroxy ligand. For the free energy of the solvating proton, the experimental number by Tissandier et al.[23] of −264 kcal mol^{-1} was used (for the free energy of 1 M proton in water, the value of −270.3 kcal mol^{-1} was used). See the Supporting Information for more details on the calculation of pK_a values.

RESULTS AND DISCUSSION

Synthesis and characterization. **1** was synthesized in one pot from readily obtained starting materials (see the Experimental Section). Complexes **2**[14] and **3**[11a] were prepared in a similar manner. Compared with dinuclear and multinuclear WOCs,[24] complexes **1**−**3** exemplify the usually simple synthetic route for mononuclear WOCs. All three complexes could be characterized unambiguously by ^{1}H NMR. It appears that, during the NMR time scale, the two axial 4-picolines of **1** are rotating freely around the Ru−N bond so that they are identical in the NMR environment and show two 4H AA′BB′ patterns of signals at 6.89 and 8.24 ppm, respectively. Additionally, the tridentate hqc ligand shows discrete proton-coupled peaks in the region of 6.6−7.8 ppm. It should be noted, in the ^{1}H NMR spectra of **1**, that the chemical shifts assigned to the protons of equatorial 4-picoline (both at the ring and at the methyl group) are more upfield than those of axial picolines, indicating a more significant electronic influence of the hqc ligand on the equatorial position rather than the axial position.

UV−vis absorption of **1** in CH_2Cl_2 at room temperature displays an intense band in the near-UV region assigned to the $\pi-\pi^*$ electron transitions of the ligands, while the band at the longer-wave region, λ_{max} = 525 nm, is associated with a metal-to-ligand charge transfer (MLCT) from a Ru d orbital to the lowest-lying π^* orbital of the ligand, hqc in this case.

X-ray-quality single crystals of **1** were obtained by the slow evaporation of its CH_2Cl_2/heptane solution, and the structure is shown in Figure 1. Single crystals of **3** were also cultivated and resolved for the purpose of comparative study. Although complex **3** had been reported before,[11a,13,25] its steric structure had not been revealed in detail yet. Selected metrical data for both **1** and **3** were summarized in Tables 1 and 2. Both complexes display distorted octahedral coordination geometries with the Ru^{II} core located in the plane of the tridentate ligand, hqc for **1** and tpy for **3**, respectively. The distance of three Ru−N(picoline) bonds of **1** falls in the range of 2.114−2.137 Å, which are generally longer than the corresponding Ru−N(picoline) bonds in **3** (2.093−2.125 Å). It should be noted that, in either **1** or **3**, the equatorial Ru−N(picoline) bond is longer than the axial one.

The major differences between the structures of **1** and **3** lie in the O-donor groups of hqc and the N-donor groups of tpy. The ruthenium carboxylate (Ru1−O1) or ruthenium phenolate (Ru1−O4) bonds are longer than the Ru−N (terpyridine) bonds (Ru1−N1 and Ru1−N3) in **3**. The angle of O1−Ru−O4

dx.doi.org/10.1021/ic201348u | *Inorg. Chem.* 2012, 51, 3388−3398

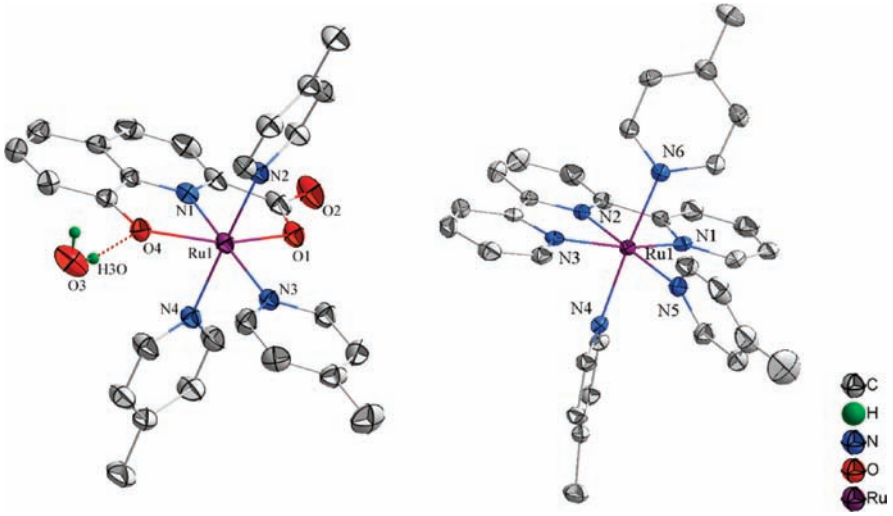

Figure 1. X-ray crystal structures of **1** (left, ellipsoids at 30% probability) and **3** (right, ellipsoids at 50% probability). H atoms (except water) and PF_6^- are omitted for clarity.

Table 1. Summary of the Crystal Data for 1 and 3

	1	3
formula	$C_{58}H_{57}C_{l4}N_8O_7Ru_2$	$C_{33}H_{32}F_{12}N_6P_2Ru$
fw	1322.06	903.66
space group	*C*2/*c*	*P*121/*c*
a/Å	17.063(4)	14.0076(14)
b/Å	13.802(4)	19.784(3)
c/Å	25.853(6)	13.5054(11)
α/deg	90.00	90.00
β/deg	95.167(14)	101.369(7)
γ/deg	90.00	90.00
V/Å^3	6064.(3)	3669.3(7)
Z	4	4
D_c/g cm^{-3}	1.449	1.636
T/K	299	173
F(000)	2692	1816
μ(Mo K*α*)/mm^{-1}	0.710 73	0.710 73
reflns collected	6927	8304
GOF on F^2	1.02	1.00
final *R* indices	0.049	0.040
R1[a] [$I > 2\sigma(I)$] (all)	0.082	0.105
wR2[b] [$I > 2\sigma(I)$] (all)	0.131	0.065

[a] $R1 = \sum(|F_o| - |F_c|)/\sum|F_o|$. [b] $wR2 = \{\sum[w(F_o^2 - F_c^2)^2]/\sum[w(F_o^2)^2]\}^{1/2}$.

Table 2. Selected Bond Distances (Å) and Angles (deg) for 1 and 3

1		3	
Bond Distances			
Ru1−N1	1.965(3)	Ru1−N1	2.081(3)
Ru1−N2	2.114(3)	Ru1−N2	1.956(2)
Ru1−N3	2.137(3)	Ru1−N3	2.087(2)
Ru1−N4	2.121(3)	Ru1−N4	2.093(3)
Ru1−O1	2.170(3)	Ru1−N5	2.125(3)
Ru1−O4	2.176(3)	Ru1−N6	2.097(3)
H30−O4	2.085		
Bond Angles			
N1−Ru1−N2	94.10	N1−Ru1−N2	79.70
N2−Ru1−N3	87.81	N2−Ru1−N3	79.39
N3−Ru1−N4	98.07	N3−Ru1−N5	101.50
N4−Ru1−N1	90.14	N5−Ru1−N1	99.41
N1−Ru1−O1	78.33	N2−Ru1−N4	92.20
O1−Ru1−N3	98.24	N4−Ru1−N5	87.74
N3−Ru1−O4	103.17	N5−Ru1−N6	89.37
O4−Ru1−N1	80.28	N6−Ru1−N2	90.66
O1−Ru1−O4	158.59	N1−Ru1−N3	159.09

in **1** is smaller than that of N1−Ru1−N3 in **3**. Notably, the hydroxyl group in **1** formed a hydrogen bond (H3O−O4) with a solvate water molecule.

Labile Picoline Ligand. Electrospray ionization mass spectrometry (ESI-MS) is a soft ionization technique that has been successfully applied by our and other groups to detect charged intermediates involved in catalytic water oxidation.[12c,26] In this work, a sample was directly injected into the MS instrument immediately after the addition of Ce^{IV} (in a pH 1.0 CF_3SO_3H aqueous solution) to a dilute solution of **1** (in acetone/water) under vigorous stirring. Usually, the moderate formula weights of mononuclear ruthenium complexes keep the appearance of their signals in a certain region of the MS spectra; meanwhile, the typical isotopic distribution of ruthenium makes these signals distinct from other charged species.

Figure 2 shows the MS spectra of **1** before and after the addition of 4 mol equiv of Ce^{IV}. The peaks of $[\mathbf{1} + H]^+$ and $[\mathbf{1} + Na]^+$ are the major signals for starting complex **1** in an acetone/water solution. After treatment with 4 equiv of Ce^{IV}, signals of $[Ru^{III}(hqc)(pic)_2 + H_2O]^+$ and $[Ru^{III}(hqc)(pic)_2 + CH_3COCH_3]^+$ emerged in the MS spectrum, besides the peaks of $[Ru^{III}(hqc)(pic)_3]^+$. This observation indicates a ligand-exchange process occurring to complex **1** under experimental water oxidation conditions, that is, replacement of one of its 4-picoline ligands with a water or acetone molecule. Considering the NMR and crystal structure discussed above, we propose that ligand exchange happens at the equatorial 4-picoline of **1**. The spectrum obtained after the addition of another 4 equiv of Ce^{IV} (8 equiv in total) does not reveal any new species but shrinkage of the $[Ru^{III}(hqc)(pic)_3]^+$ and $[Ru^{III}(hqc)(pic)_2 + CH_3COCH_3]^+$ signals and enhancement of the $[Ru^{III}(hqc)(pic)_2 + H_2O]^+$ signal. The formation of ruthenium(IV) and ruthenium(V) species is expected under the experimental conditions, whose lifetimes, however, are too short to be captured by the MS.

The geometry of $[Ru^{III}(hqc)(pic)_2OH_2]^+$ was optimized using DFT with additional explicit water molecules (Figure 3)

dx.doi.org/10.1021/ic201348u | Inorg. Chem. 2012, 51, 3388−3398

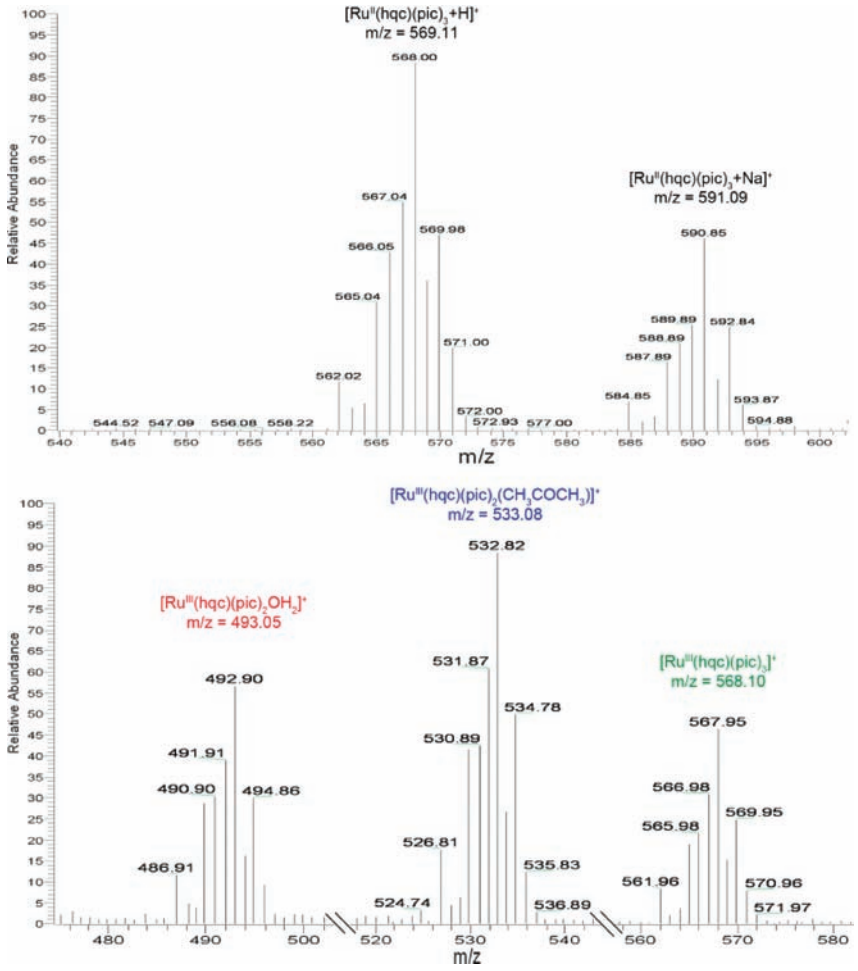

Figure 2. ESI-MS spectra (positive mode) of **1** in acetone/water (1:9) before (top) and after (bottom) the treatment of 4 equiv of $Ce^{IV}(Ce(NH_4)_2(NO_3)_6$ in a pH 1.0 CF_3SO_3H aqueous solution).

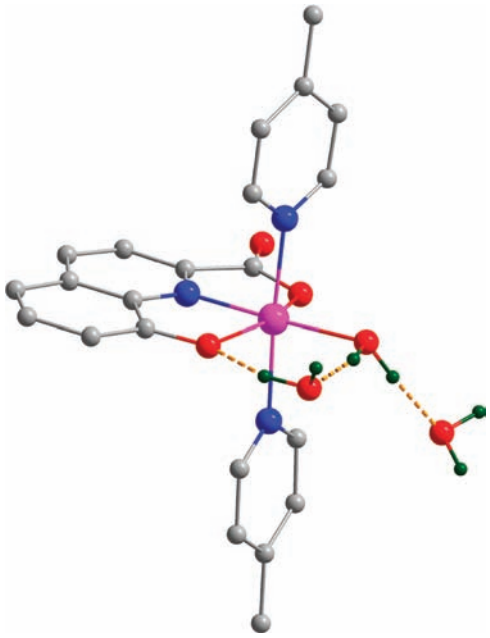

Figure 3. Calculated geometry of $[Ru^{III}(hqc)(pic)_2OH_2]^+$ in an aqueous medium. H atoms except those bonding to O atoms are omitted for clarity. Color code: purple, Ru; blue, N; red, O; gray, C; green, H.

in order to reproduce precisely the strong protic solvation in a realistic medium (see the Supporting Information). One of the explicit water molecules acts both as a hydrogen-bond acceptor to the aqua ligand of $[Ru^{III}(hqc)(pic)_2OH_2]^+$ and as a hydrogen-bond donor to the phenol O atom. These hydrogen bonds are reminiscent of the hydrogen-bonding network in PSII surrounding the Mn_4CaO_5 cluster, which may function as a channel for proton transfer and assist in the PCET process.[27]

The formation of the corresponding $Ru^{III}OH_2$ species via fast ligand substitution was also observed for complex **2** under the same Ce^{IV}/CF_3SO_3H conditions.[14] However, the reaction did not proceed for **3** at such a high rate.[13] Even if 16 equiv of Ce^{IV} was added to the solution of **3**, neither $Ru^{III}OH_2$ nor $Ru^{III}CH_3COCH_3$ peaks were recorded by MS spectroscopy. To understand how the tridentate ligand affects the ligand-exchange processes, we performed a theoretical study on these reactions.

Complexes $Ru^{II}(L)(pic)_3$ (L = hqc for **1**, pdc for **2**, and tpy for **3**) were examined as the starting point of our DFT calculation. The redox potentials of $Ru^{III}(L)(pic)_3/Ru^{II}(L)(pic)_3$ were calculated to be 0.29 V (**1**), 0.6 V (**2**), and 1.4 V (**3**) vs NHE, respectively, which are consistent with the experimental values (vide infra). For complexes **1** and **2**, which contain anionic ligands, this oxidation step is postulated to occur rapidly. Because the oxidative potential of Ce^{IV} at pH 1.0 is >1.5 V vs NHE, complex **3** is likely to be oxidized to the Ru^{III} state as well under

dx.doi.org/10.1021/ic201348u | Inorg. Chem. 2012, 51, 3388–3398

the typical O_2-evolving experimental conditions, despite its higher redox potential.

Two possible mechanistic scenarios were considered for the $Ru^{III}(L)(pic)_3 \rightarrow Ru^{III}(L)(OH_2)(pic)_2$ reaction. One is the concerted associative pathway (route a in Scheme 2), where a

Scheme 2. (a) Associative and (b) Dissociative Ligand-Exchange Pathways

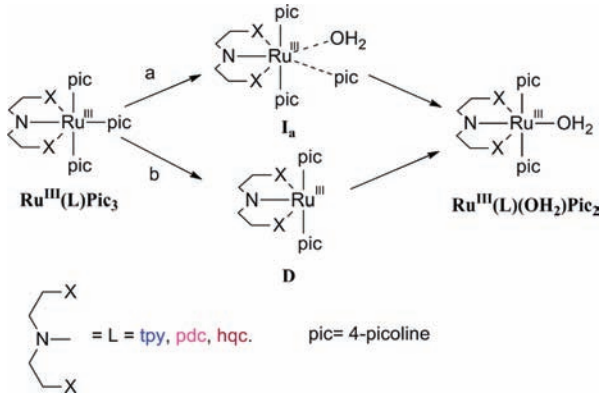

water molecule enters the coordination sphere of $Ru^{III}(L)(pic)_3$ simultaneously with the departure of a 4-picoline ligand (the transition state is labeled as I_a); the other is the dissociative pathway (route b in Scheme 2), where a picoline ligand dissociates from $Ru^{III}(L)(pic)_3$ first, giving a five-coordinated ruthenium(III) intermediate (the intermediate is labeled as **D**), followed by coordination of a water molecule. The energy profiles of the two pathways are outlined in Figure 4.

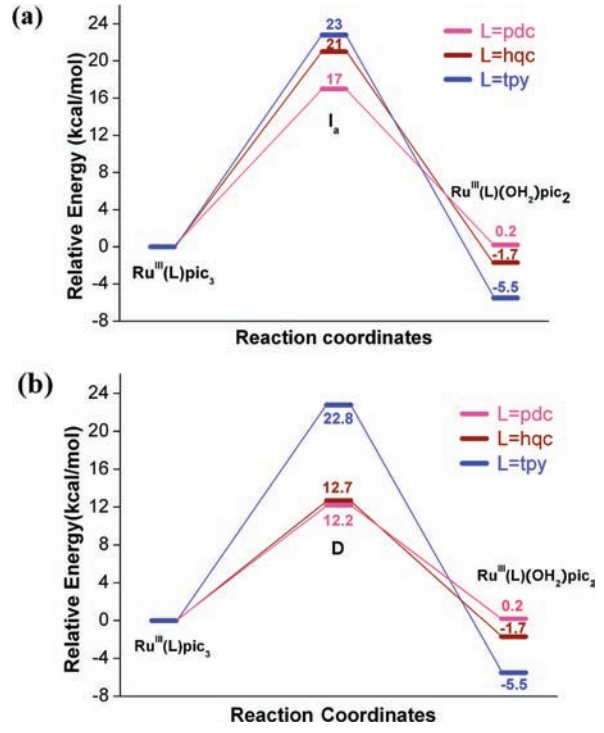

Figure 4. (a) Reaction coordinate of the associative ligand exchange. (b) Reaction coordinate of the dissociative ligand exchange via the five-coordinated intermediate **D**.

In either situation, catalyst **3** with a neutral tpy ligand has the highest activation energy. While the free energies of I_a and **D** for catalyst **3** are almost identical (23.0 kcal mol^{-1} for I_a and 22.8 kcal mol^{-1} for **D**), for complexes **1** and **2** bearing anionic ligands, the free energies of **D** in the dissociative pathway are much lower than those of I_a in the concerted associative pathway, indicating the dissociative pathway as the dominate picoline/OH_2 exchange mechanism. It was previously reported that water dissociation from a dinuclear ruthenium(III) complex with oxygen ligands proceeds via a dissociative mechanism;[28] however, water association simultaneous with dissociation of picoline through an interexchange pathway has also been found for other ruthenium(III) systems and cannot be excluded in our case.[29] It should be noted that the required energy of picoline dissociation for **1** or **2** (merely 12.7 and 12.2 kcal mol^{-1}, respectively) is roughly half of the corresponding value for **3**.

DFT calculations of the ligand-exchange mechanism confirmed the experimental observation that complexes **1** and **2** undergo rapid picoline/OH_2 exchange at the Ru^{III} state. On the contrary, the low picoline/OH_2 exchange rate of **3** conspicuously impedes generation of the $Ru^{III}OH_2$ intermediate, which is a necessary initial species in the catalytic circle of water oxidation.

We note that the lowest unoccupied molecular orbital (LUMO) of **D** (the LUMO is the orbital that the dissociated 4-picoline binds to) is similar in all three complexes and is mainly composed of the d_{z^2} orbital of ruthenium. However, the calculated LUMO energy of **D** for **3** shows a significantly lower value of −0.134 au compared to the corresponding values for **1** and **2**, which are −0.093 and −0.094 au, respectively. This implies that stabilization of the binding of a dative ligand, such as 4-picoline, to **3** is greater, and therefore the Ru−N bond is less labile and less reactive. Interestingly, natural population analysis (NPA; Table 3) shows that the partial charge at the Ru center

Table 3. NPA of D

	$Ru^{III}(L)(pic)_2$ (**D**)		
	L = tpy	L = pdc	L = hqc
charge of Ru	0.9829	1.1179	1.0531

of complex **3** is less positive than those of complexes **1** and **2**. This result indicates that the influence of the electrostatic force is not as large as that of the orbital interaction because the picoline binds less strongly to the complex where the partial charge at ruthenium is larger. The orbital energies are outlined in Figure 5.

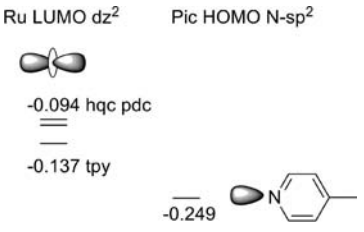

Figure 5. Interacting orbitals of dative ligand 4-picoline and ruthenium(III) intermediates (**D**).

Electrochemical Study. The electrochemical behavior of complex **1** was first evaluated in an organic medium, as shown in Figure 6, in which the cyclic voltammograms of **2** and **3** are also displayed. Apparently, the properties of ligands significantly influence the redox potential of **1**−**3**, leading to the dramatically lower $E_{1/2}$ (Ru^{III}/Ru^{II}) of **1** and **2** containing anionic ligands in

dx.doi.org/10.1021/ic201348u | Inorg. Chem. 2012, 51, 3388−3398

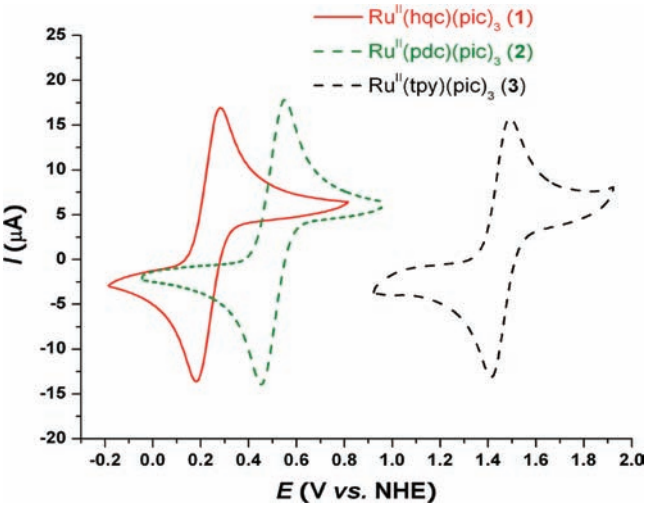

Figure 6. CV curves of complexes **1**−**3** in organic solvents.

comparison with that of **3** containing a neutral ligand. Moreover, $E_{1/2}(Ru^{III}/Ru^{II})$ of **1** appears at 0.23 V vs NHE, which is 0.27 V less positive than the corresponding potential of **2**. The lower potential is likely due to the better π-electron-donating ability of the phenol group compared to that of the carboxylate group.

The electrochemical properties of **1**−**3** were further investigated in both neutral and acidic aqueous solutions (Figures S4 and S5 in the Supporting Information). In pH 7.0 phosphate buffers, catalytic water oxidation by **1** occurred along with the onset of a rapid increase in the current at around 1.05 V vs NHE, while the catalytic onset for **2** was observed at 1.26 V vs NHE.[14] Thus, the phenol donor further decreases the catalytic overpotential, compared to the carboxylate donor. The different catalytic onsets between **1** and **2** demonstrate that an anionic ligand plays a key role in the overall electron density of the complex not only at the low-valent state of the Ru center, Ru^{II} or Ru^{III}, but also at the high-valent state of the metal core, which is directly related to the rate-determining step in water oxidation catalysis. In a neutral medium, the catalytic potential of **1** is lower than $E_{1/2}(Ru^{III}/Ru^{II})$ of $[Ru(bpy)_3]^{2+}$, presenting the possibility of applying **1** into visible-light-driven water oxidation, coupled with $[Ru(bpy)_3]^{2+}$ types of PSs. In pH 1.0 CF_3SO_3H solutions, the observed catalytic onsets of **1** and **2** are very close to each other.

Specific waves in the CVs of **1**−**3** are included in Table 4. It has been shown in our previous work that $Ru^{II}(tpy)(pic)_2(H_2O)$ is an active WOC, which displays a catalytic wave in its CV curves.[13] The absence of a catalytic onset for **3** in an aqueous solution verified our conclusion from the ESI-MS spectra and DFT study above that ligand exchange between 4-picoline and water does not occur to **3** as readily as it does to **1** and **2**.

Because complexes **1** and **2** are insoluble in water, the addition of an organic cosolvent (typically acetonitrile or acetone) is unavoidable for electrochemical measurement in an aqueous solution. The acetonitrile (or acetone) molecule, however, is able to substitute coordinated water, leading to the formation of Ru−solvent species as shown in the MS spectra (equilibrium between $Ru-OH_2$ and Ru−solvent is expected). Although the existence of Ru−solvent species does not affect the catalytic water oxidation because only aquaruthenium species can reach the high-valent state (e.g., Ru^V) via PCET, the redox waves of Ru−solvent, as well as waves of the original Ru−pic complexes, strongly interfere with identification of the redox waves of aquaruthenium intermediates that formed in situ during voltammetric scanning. In order to further illustrate the eletrochemical properties of aquaruthenium intermediates, we proceeded with DFT modeling of a sequence of PCET pathways based on complexes **1**−**3** from the Ru^{III} to Ru^V state (Scheme 3).[7,12]

Table 4. Selected CV Data for Complexes 1−3.[a]

complex	$E_{1/2}(Ru^{III}/Ru^{II})$ organic solvents[b]	catalytic onset at pH 7.0[c]	catalytic onset at pH 1.0[d]
1	0.23	1.05	1.51
2	0.50[e]	1.26[e]	1.53[e]
3	1.45	*f*	*f*

[a]All potential values were given vs NHE; $E_{1/2} = (E_{pa} + E_{pc})/2$, and the complex is regarded to catalyze water oxidation when the scanned current is obviously higher than that of the background; the concentration of sample is 1 mM, and the scan rate is 100 mV s^{-1}. [b]0.1 M Bu_4NPF_6 in CH_2Cl_2 (**1** and **2**) or CH_3CN (**3**) was used as the electrolyte, and ferrocene (Fe^{III}/Fe^{II} = 0.63 V vs NHE) was used as the external reference. [c]pH 7.0 phosphate buffer (50 mM) containing 10% acetonitrile. [d]Aqueous solution of CF_3SO_3H (pH 1.0) containing 10% acetonitrile; $Ru^{II}(bpy)_3Cl_2$ (Ru^{III}/Ru^{II} = 1.26 V vs NHE) was used as the external reference in both pH 1.0 and pH 7.0 aqueous media. [e]The data are from previous work.[14] [f]Not observed.[13]

Scheme 3. Calculated Redox Potentials of $RuOH_2$ Complexes at pH 0 and 7.0

pH = 7.0

complex **1**: $Ru^{III}(hqc)$-OH $\xrightarrow{0.78\ eV}$ $Ru^{IV}(hqc)$=O $\xrightarrow{1.23\ eV}$ $[Ru^{V}(hqc)=O]^+$

complex **2**: $Ru^{III}(pdc)$-OH $\xrightarrow{0.78\ eV}$ $Ru^{IV}(pdc)$=O $\xrightarrow{1.38\ eV}$ $[Ru^{V}(pdc)=O]^+$

pH = 0

complex **1**: $[Ru^{III}(hqc)-OH_2]^+$ $\xrightarrow{1.35\ eV}$ $[Ru^{IV}(hqc)-OH]^+$ $\xrightarrow{1.49\ eV}$ $[Ru^{V}(hqc)=O]^+$

complex **2**: $[Ru^{III}(pdc)-OH_2]^+$ $\xrightarrow{1.50\ eV}$ $Ru^{IV}(pdc)$=O $\xrightarrow{1.38\ eV}$ $[Ru^{V}(pdc)=O]^+$

The pK_{a1} values of $[Ru^{III}(hqc)OH_2]^+$ and $[Ru^{III}(pdc)OH_2]^+$ were calculated as 7.0 and 5.2, respectively. The pK_a value of $[Ru^{IV}(hqc)OH]^+$ was calculated as 4.4 and that of $[Ru^{IV}(pdc)OH]^+$ as −0.1, which reflects the higher electron density at ruthenium when bonded to a hqc ligand. All of these computed pK_a values are summarized in Table 5. The pK_{a1} values of $[Ru^{III}(tpy)OH_2]^{3+}$ and $[Ru^{IV}(tpy)OH]^{3+}$ are also given for comparison.

Table 5. Calculated pK_a Values

	L = tpy	L = pdc	L = hqc
$Ru^{III}(L)OH_2$ (pK_{a1})	−0.4	5.2	7.0
$Ru^{IV}(L)OH$ (pK_a)	−8.1	−0.1	4.4

The calculated redox potentials of aquaruthenium(III) complexes (Scheme 3) show a significant dependence on the pH values. At pH 0, PCET yields $[Ru^{IV}(hqc)OH]^+$ from $[Ru^{III}(hqc)-OH_2]^+$, while the $Ru^{IV}(pdc)$=O complex is the most stable form from oxidation of $[Ru^{III}(pdc)OH_2]^+$ because of the different pK_a values of the corresponding ruthenium(IV) species. The calculated potential is 1.35 V for the Ru(hqc) couple and 1.5 V for the Ru(pdc) couple. At pH 7.0, both complexes are oxidized to the Ru^{IV}=O intermediates from $Ru^{III}OH$ forms and both complex couples have the same redox potential of 0.78 V. The lower Ru^{IV}/Ru^{III} redox potential at pH 7.0 is likely due to more facile deprotonation of the aquaruthenium(III) complexes. It is very interesting that at pH 7.0 the ligand effect is functioning in two

dx.doi.org/10.1021/ic201348u | Inorg. Chem. 2012, 51, 3388−3398

counteracting ways on the redox potentials. The electron-rich hqc ligand makes deprotonation of the Ru^{III}(hqc)OH complex less facile compared to that of the Ru^{III}(pdc)OH complex, but it also stabilizes the high-valence Ru^{IV}=O state. The result is that the Ru^{IV}/Ru^{III} redox potentials are calculated as identical for the two complex couples.

Because the phenolate ligand is a stronger π-donating donor than the carboxylate ligand, the calculated redox potential of a single-electron Ru^{IV}(hqc)=O/$[Ru^{V}$(hqc)=O$]^+$ process is 0.15 V more negative than that of Ru^{IV}(pdc)=O/$[Ru^{V}$(pdc)=O$]^+$ at pH 7.0. The highest occupied molecular orbital (HOMO) energies were calculated as −0.205 and −0.222 au for Ru^{IV}(hqc)=O and Ru^{IV}(pdc)=O, respectively. At pH 0, however, suppression of PCET leads to a more positive redox potential of $[Ru^{IV}$(hqc)-OH$]^+/[Ru^{V}$(hqc)=O$]^+$ (1.49 V vs NHE) than that of Ru^{IV}(pdc)=O/$[Ru^{V}$(pdc)=O$]^+$ (1.38 V vs NHE). Considering that the catalytic onsets observed in the electrochemical experiment (Table 4) are very close to the calculated redox potentials of $[Ru^{V}$(L)=O$]^+$ formation (L = hqc or pdc), we propose that both $[Ru^{V}$(hqc)=O$]^+$ and $[Ru^{V}$(pdc)=O$]^+$ react with water directly and undergo O−O bond formation readily, although nucleophilic attack of water to other high-valent Ru−oxo intermediates cannot be completely ruled out.

Ce^{IV}-Driven Water Oxidation. Under typical Ce^{IV}-driven water oxidation conditions, O_2 was generated immediately and continuously after **1** was injected into the Ce^{IV}/CF_3SO_3H solution (initial pH 1.0), as reflected by the response of a fluorescent oxygen probe positioned in the headspace of the reaction vessel. After 12 h, the amount of evolved O_2 was calibrated by GC and a turnover number (TON) of 680 was achieved (Figure S6 in the Supporting Information). Rapid O_2 evolution was also observed when **2** was added into a Ce^{IV}/CF_3SO_3H solution.[14] It is, however, not the situation for complex **3**, which undergoes a long period of induction time (about 2 h) before evolved O_2 could be detected.[13] According to the different catalytic behaviors of **1**−**3** and the essential outcomes from experimental and theoretical discussions above, we propose that (i) 4-picoline to water ligand exchange, the formation of $Ru^{III}OH_2$, is required as an initiative process for water oxidation catalyzed by **1**−**3** and (ii) the difficult dissociation of 4-picoline ligand suppresses the catalytic activity of **3**, while ligand exchange occurs easily for **1** and **2** and does not impose any detrimental influence on their catalytic rate. A similar H_2O/Cl^- ligand exchange that involved water oxidation catalysis has been reported for other mononuclear ruthenium complexes.[11b]

The kinetics of Ce^{IV}-driven water oxidation catalyzed by **1** was first studied by monitoring the initial absorbance decay of Ce^{IV} at 360 nm after mixing the catalyst with Ce^{IV}/CF_3SO_3H solutions. Spectrophotometric research reveals a predominant catalytic pathway for **1**, which follows a zero-order dependence in the concentration of Ce^{IV} (Figure S7 in the Supporting Information; $[Ce^{IV}]$ > 100 equiv) and a first-order dependence in the concentration of catalyst (rate = k[**1**]; Figure 7). This result indicates, on the one hand, that **1** probably catalyzes water oxidation through a water nucleophilic attack mechanism proposed by Meyer et al.[12] and Ce^{IV} is not associated with the rate-determining step of the catalytic cycle when the concentration of Ce^{IV} is much higher than that of catalyst. On the other hand, the determined reaction rate constant, k, is 1.42 s^{-1} for **1**, which is several orders of magnitude higher than those of extensively studied mononuclear aquaruthenium WOCs with neutral polypyridyl ligands.[12] The remarkably high catalytic activity was also shared by complex **2** (k was determined as 1.36 s^{-1} under

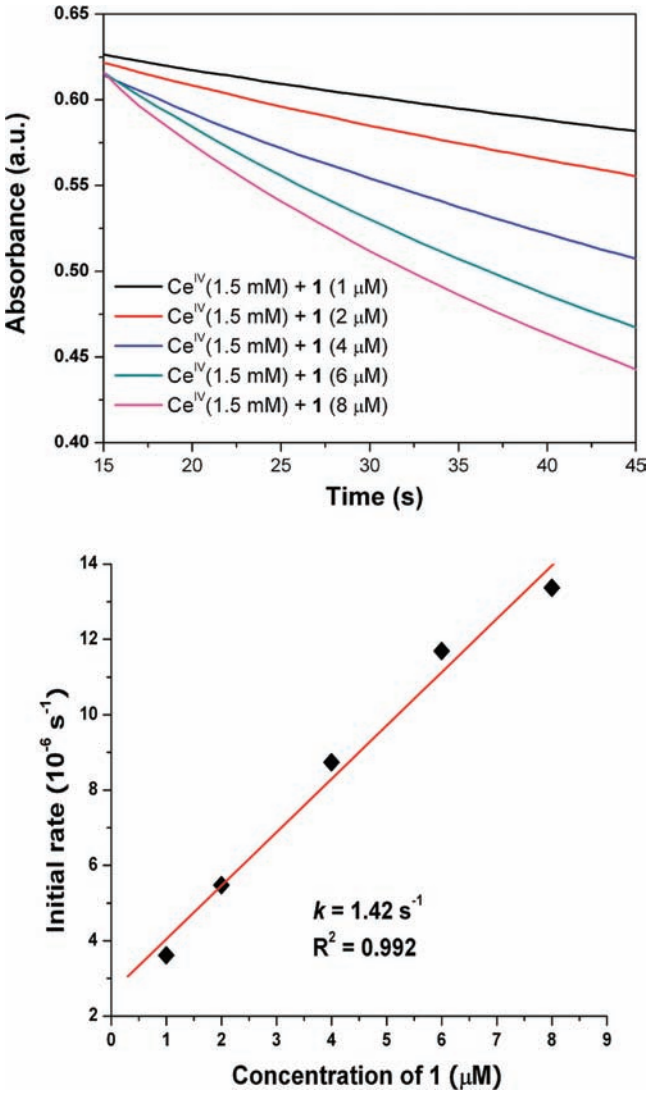

Figure 7. Top: Absorption change of Ce^{IV} monitored at 360 nm after the addition of complex **1** (1, 2, 4, 6, and 8 μM) into a Ce^{IV} aqueous solution (1.5 mM, pH 1.0). The initial rate was calculated by taking the first 30 s spectral decay as linear. No data were collected in the first ca. 15 s because of the operation for injecting the catalyst and mixing the solution. Bottom: Determination of k as a function of the concentration of **1**.

similar experimental conditions),[14] implying that the given anionic ligands decrease the energy barrier of the rate-determining step in the overall water oxidation cycle.

Moreover, the catalytic rate constant of O_2 evolution (k_{O_2}) was also measured (Figure 8) using pressure transducers. As expected, a linear relationship between the initial O_2-evolving rate and the concentration of **1** was observed and follows an expression of pseudo-first-order reaction rate = k_{O2}[**1**] (the Ce^{IV} used in the measurement is larger excess, >4000 equiv, and can be regarded as constant). The TOF of **1** calculated from k_{O_2} is 0.32 s^{-1}, which renders **1** as one of the most efficient mononuclear ruthenium WOCs ever reported (the TOF of **2** is 0.23 s^{-1}).[14]

Visible-Light-Driven Water Oxidation. Taking its advantage of low catalytic overpotential, complex **1** also functions in a homogeneous light-driven water oxidation system that consists of three components: catalyst, PS, and sacrificial electron acceptor

dx.doi.org/10.1021/ic201348u | Inorg. Chem. 2012, 51, 3388−3398

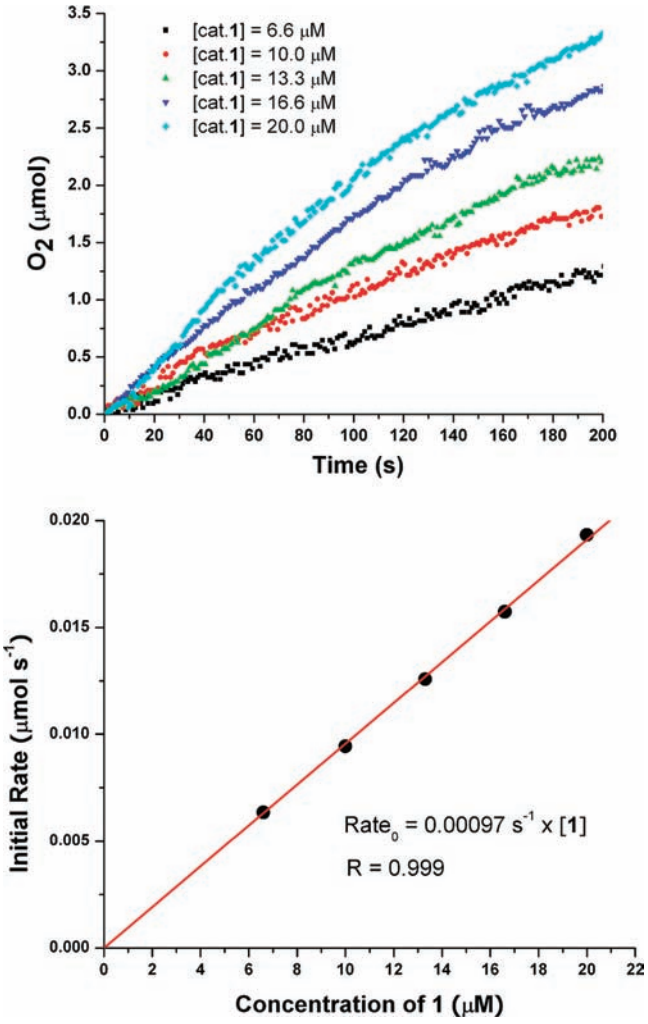

Figure 8. Top: Plots of O_2 evolution versus time at various concentrations of catalyst **1**: 6.6 μM (black ■), 10.0 μM (red ●), 13.3 μM (green ▲), 16.6 μM (blue ▼), and 20 μM (light-blue ◆) in a CF_3SO_3H aqueous solution (initial pH 1.0, 3 mL) containing Ce^{IV} (0.083 M). The initial rates were calculated by fitting the O_2 versus time curves from 0 to 150 s as a straight line. Bottom: Determination of k_{O_2} by plotting the initial rate of O_2 generation against the concentration of **1**.

(illustrated in Scheme 4). Besides commonly used $[Ru(bpy)_3]^{2+}$ (**P1**), another two analogues, $[Ru(bpy)_2(dcbpy)]^{2+}$ [**P2**; dcbpy = 4,4′-bis(ethoxycarbonly)-2,2′-bipyridine] and $[Ru(bpy)(dcbpy)_2]^{2+}$ (**P3**), were also employed as PSs in this work. Their redox potentials $[E([Ru^{3+}/Ru^{2+}])]$ are summarized in Table 6. All of these PSs (**P1**–**P3**) have typical MLCT

Scheme 4. Mechanism for Visible-Light-Driven Water Oxidation by Complex 1 Using $[Ru(bpy)_3]^{2+}$ PSs (P1) and a Persulfate Acceptor

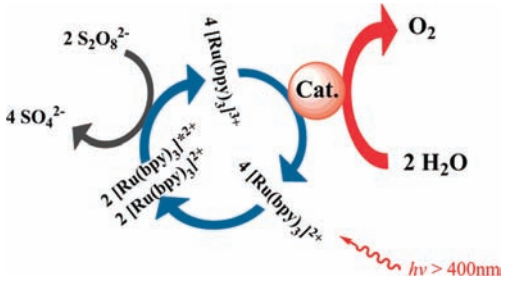

Table 6. Oxidation Potentials of PSs and Light-Driven Water Oxidation by 1[a]

	P1	P2	P3
$E(Ru^{3+}/Ru^{2+})$ vs NHE (V)[b]	1.26	1.37	1.50
TON of **1**[c]	<5	42	61
TOF of **1** (min^{-1})[d]	<1	2.7	3.0

[a]TONs and TOFs of **1** were calculated according to Figure 6. [b]In phosphate buffer (50 mM, pH 7.0). [c]After 52 min. [d]The TOF was calculated as the slope of linearly fitted O_2 evolution plots in the period of 0–12 min.

absorbance in the visible-light region (λ > 400 nm). Persulfate, $S_2O_8^{2-}$, was used as the sacrificial electron acceptor to quench excited PS (PS*) in this photocatalytic system. The generated $SO_4^{\bullet-}$ from photooxidation is an even stronger oxidant and can continue to oxidize one more unexcited PS to PS^+.[30] Overall, the absorption of two photons and the consumption of 2 equiv of $S_2O_8^{2-}$ afford four PS^+ (eq1), which sequentially oxidize 2 equiv of H_2O to O_2 under catalysis of **1** (eq 2).

$$4PS + 2S_2O_8^{2-} + 2h\nu \rightarrow 4PS^+ + 4SO_4^{2-} \quad (1)$$

$$4PS^+ + 2H_2O \rightarrow 4PS + O_2 + 4H^+ \quad (2)$$

Figure 9 describes O_2-evolving plots versus the illumination time, when complex **1** was assembled with PSs **P1**–**P3**, respectively.

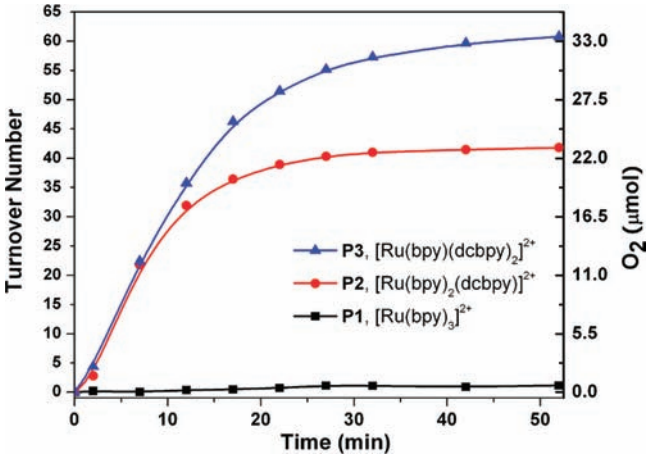

Figure 9. Plot of O_2 evolution versus the illumination time in a three-component light-driven water oxidation system. All data were measured by GC. Conditions: a xenon lamp (500 W) with a λ > 400 nm filter, 10 mL of pH 7.2 phosphate buffer (20 mM), 0.55 mL of acetonitrile, [**1**] = 55.0 μM, [**P1**]–[**P3**] = 550 μM, and [$S_2O_8^{2-}$] = 10 mM.

The O_2 concentration in the reactor was monitered by automatically pumping a small amount of gas from the headspace of the reactor to the gas chromatograph every 5 min. Integrated with **P1**, complex **1** can achieve light-driven water oxidation in the described system; the detected TON and TOF, however, were low. That is probably because the difference between the oxidation potential of **P1** and the catalytic potential of **1** is not large enough to efficiently drive electron transfer from the catalyst to the PS. While **P2** or **P3** was employed as the PS, whose $E(Ru^{3+}/Ru^{2+})$ is 0.11–0.24 V higher than that of **P1**, fast O_2 evolution was observed under illumination with high TOFs

dx.doi.org/10.1021/ic201348u | Inorg. Chem. 2012, 51, 3388–3398

up to 3.0 min^{-1}. The corresponding TONs and TOFs are included in Table 6. Control experiments with $RuCl_3$ or $Ru(bpy)_2Cl_2$ as a substitute for **1** did not show any O_2 evolving under the same experimental conditions, confirming the photocatalytic process as that depicted in Scheme 4.

We reported the sharp drop of the pH in the process of light-driven water oxidation in our earlier work,[31] which could explain the depressed O_2 generation rate after about 20 min of illumination, as shown in Figure 9. Aiming at an insight into the pH effect, we repeated the **1**−**P3**−$S_2O_8^{2-}$ light-driven water oxidation by employing a Clark electrode detector, which is very sensitive to the change of the O_2 concentration in the liquid phase. As displayed in Figure 10, the pH of the buffer solution

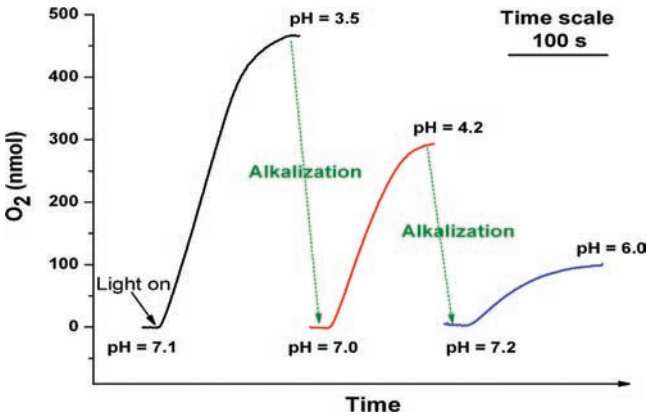

Figure 10. Repetitive light-driven water oxidation reaction. Conditions: 2 mL of phosphate buffer (initial pH 7.1, 8.3 mM) containing $Na_2S_2O_8$ (1×10^{-2} M), $[Ru(bpy)(dcbpy)_2]Cl_2$ (**P3**; 1×10^{-3} M), and complex **1** (1×10^{-5} M). A sodium hydroxide aqueous solution (0.25 M) was used for alkalization.

decreased from 7.1 initially to 3.5 at the end, along with the ceasing of light-driven O_2 generation. When the deactivated solution (pH 3.5) was neutralized to 7.0 with a sodium hydroxide aqueous solution and irradiated, O_2 evolution could be recovered again. The repeatable O_2-evolving course by alkalization correlates how the AP system is deactivated by the enhanced acidity of the medium. The gradual shrinkage of O_2 evolution in the sequential alkalization runs (Figure 10) is mainly attributed to the decomposition of PSs. The excited PSs are vulnerable in the O_2-rich $S_2O_8^{2-}$ solution when electron transfer from WOCs to PSs is suppressed under low-pH conditions.

Because the catalytic potentials of WOCs are rising along with decreasing pH, either **P2** or **P3** tends to lose its capability of triggering O_2 evolution as the reaction proceeds. However, we can see from Figure 9 that **P3**, rather than **P2**, can work in a more acidic medium and achieve a higher TON because of its higher oxidation potential $E(Ru^{3+}/Ru^{2+})$.

The photon-to-O_2 generation quantum yield, Φ, defined as the number of oxidized H_2O molecules ($^1/_2$ evolved O_2) per photon absorbed (eq 3), was measured as 9% for the **1**−**P3**−$S_2O_8^{2-}$ catalytic system. The number of O_2 molecules evolved can be calculated from the amount of generated O_2 measured by GC. The number of photons absorbed can be calculated by eq 4, where n_p is the moles of photons absorbed, I is the radiant power of input light, I_o is the radiant power of output light (in our case $I_o = 0$), λ is the wavelength of the light, t is the irradiation time, h is Planck's constant, N_A is Avogadro's constant, c is the speed of light, and ρ is the reflectance of the air/reaction vessel interface, which was measured as 9% in our experiment. The relatively low quantum yield is ascribed to the inefficiency of generating Ru^{3+} PSs and low reaction rate between PSs and catalysts.[32]

$$\Phi = 2 \times \text{number of } O_2 \text{ molecules evolved} / \text{number of photons absorbed} \quad (3)$$

$$n_p = \frac{(1-\rho)(I-I_o)t\lambda}{N_A hc} \quad (4)$$

CONCLUSIONS

In conclusion, a novel mononuclear ruthenium catalyst **1** has been prepared and thoroughly characterized that can catalyze water oxidation in a homogeneous visible-light-driven system. When cerium(IV) is employed as the oxidant, a high TOF of 0.32 s^{-1} is achieved by **1**. A comparative study of this suite of complexes **1**−**3** provides the opportunity to assess how anionic ligands influence the catalytic behaviors of WOCs. An important finding is that, compared with a neutral tridentate ligand like tpy, anionic tridentate ligands (hqc and pdc, for example) dramatically increase the rate of picoline/water ligand substitution, when catalysts are oxidized to the Ru^{III} state. Theoretical results suggest that the ligand exchange happens via a dissociative mechanism and negatively charged O donors, such as carboxylate and phenolate, labilize the Ru^{III}−N(pic) bond. Meanwhile, mononuclear ruthenium complexes containing anionic ligands show a much better catalytic performance than those with a neutral polypyridyl ligand. Mechanistic studies based on one-site water oxidation have provided evidence that the release of O_2 from the metal site could be rate-limiting in the overall O_2 evolution.[12] It is plausible that anionic ligands facilitate O_2 evolution by destabilizing the Ru−O_2 bond in a way that they affect the Ru−N(pic) bond. An extensive study of the anionic ligand effect on the O−O bond formation and O_2 release is under investigation.

Combined experimental and theoretical studies illustrated the diverging effects of anionic ligands on the access of Ru^{V}=O species. While it can promote the HOMO of ruthenium complexes, an anionic ligand may compromise PCET in certain circumstances. These findings demonstrate a correlation between the activity of WOCs and the properties of ligands, providing critical information for the design of highly efficient WOCs in the future. The low catalytic overpotential of complex **1** allowed visible-light-driven water oxidation, indicating the possibility of assembling **1** in a photovoltaic device for the overall water splitting.

ASSOCIATED CONTENT

Supporting Information

X-ray crystallographic data in CIF format, ^{1}H NMR and UV−vis spectra, CV curves, plot of O_2 evolution versus time, absorption changes, optimized geometries, a comparison of calculated and experimental pK_a values, Cartesian coordinates, and experimental and computational details. This material is available free of charge via the Internet at http://pubs.acs.org.

AUTHOR INFORMATION

Corresponding Author

*E-mail: mahlquist@theochem.kth.se (M.S.G.A.), lichengs@kth.se (L.S.). Tel: +46-8-7908127 (L.S.). Fax: +46-8-7912333 (L.S.).

Notes

The authors declare no competing financial interest.

■ ACKNOWLEDGMENTS

We thank the Swedish Research Council, the K&A Wallenberg Foundation, the Swedish Energy Agency, the China Scholarship Council, the National Science Foundation of China (Grant 20633020), and the National Basic Reseach Program of China (Grant 2009CB220009) for financial support of this work. All computations were performed at the PDC supercomputer center at KTH.

■ REFERENCES

(1) (a) Barber, J. *Chem. Soc. Rev.* **2009**, *38*, 185−196. (b) Dau, H.; Zaharieva, I. *Acc. Chem. Res.* **2009**, *42*, 1861−1870.
(2) Sala, X.; Romero, I.; Rodríuez, M.; Escriche, L.; Llobet, A. *Angew. Chem., Int. Ed.* **2009**, *48*, 2842−2852.
(3) (a) Alstrum-Acevedo, J. H.; Brennaman, M. K.; Meyer, T. J. *Inorg. Chem.* **2005**, *44*, 6802−6827. (b) Youngblood, W. J.; Lee, S.-H. A.; Maeda, K.; Mallouk, T. E. *Acc. Chem. Res.* **2009**, *42*, 1966−1973.
(4) Duan, L.; Tong, L.; Xu, Y.; Sun, L. *Energy Environ. Sci.* **2011**, *4*, 3296−3313.
(5) Dau, H.; Limberg, C.; Reier, T.; Risch, M.; Roggan, S.; Strasser, P. *ChemCatChem* **2010**, *2*, 724−761.
(6) Brillet, J.; Cornuz, M.; Formal, F. L.; Yum, J.; Grätzel, M.; Sivula, K. *J. Mater. Res.* **2010**, *25*, 17−24.
(7) Romain, S.; Vigara, L.; Llobet, A. *Acc. Chem. Res.* **2009**, *42*, 1944−1953.
(8) (a) Gersten, S. W.; Samuels, G. J.; Meyer, T. J. *J. Am. Chem. Soc.* **1982**, *104*, 4029−4030. (b) Gilbert, J. A.; Eggleston, D. S.; Murphy, W. R.; Geselowitz, D. A.; Gersten, S. W.; Hodgson, D. J.; Meyer, T. J. *J. Am. Chem. Soc.* **1985**, *107*, 3855−3864.
(9) Meyer, T. J.; Huynh, M. H. V. *Inorg. Chem.* **2003**, *42*, 8140−8160.
(10) Zong, R.; Thummel, R. P. *J. Am. Chem. Soc.* **2005**, *127*, 12802−12803.
(11) (a) Tseng, H.-W.; Zong, R.; Muckerman, J. T.; Thummel, R. *Inorg. Chem.* **2008**, *47*, 11763−11773. (b) Masaoka, S.; Sakai, K. *Chem. Lett.* **2009**, *38*, 182−183. (c) Wasylenko, D. J.; Ganesamoorthy, C.; Koivisto, B. D.; Henderson, M. A.; Berlinguette, C. P. *Inorg. Chem.* **2010**, *49*, 2202−2209. (d) Concepcion, J. J.; Jurss, J. W.; Brennaman, M. K.; Hoertz, P. G.; Patrocinio, A. O. T.; Murakami Iha, N. Y.; Templeton, J. L.; Meyer, T. J. *Acc. Chem. Res.* **2009**, *42*, 1954−1965.
(12) (a) Concepcion, J. J.; Jurss, J. W.; Templeton, J. L.; Meyer, T. J. *J. Am. Chem. Soc.* **2008**, *130*, 16462−16463. (b) Wang, L.-P.; Wu, Q.; Van Voorhis, T. *Inorg. Chem.* **2010**, *49*, 4543−4553. (c) Wasylenko, D. J.; Ganesamoorthy, C.; Henderson, M. A.; Koivisto, B. D.; Osthoff, H. D.; Berlinguette, C. P. *J. Am. Chem. Soc.* **2010**, *132*, 16094−16106.
(13) Duan, L.; Xu, Y.; Tong, L.; Sun, L. *ChemSusChem* **2011**, *4*, 238−244.
(14) Duan, L.; Xu, Y.; Gorlov, M.; Tong, L.; Andersson, S.; Sun, L. *Chem.—Eur. J.* **2010**, *16*, 4659−4668.
(15) Xu, Y.; Fischer, A.; Duan, L.; Tong, L.; Gabrielsson, E.; Åkermark, B.; Sun, L. *Angew. Chem., Int. Ed.* **2010**, *49*, 8934−8937.
(16) Duliere, E.; Devillers, M.; Marchand-Brynaert, J. *Organometallics* **2003**, *22*, 804−811.
(17) Elliott, C. M.; Hershenhart, E. J. *J. Am. Chem. Soc.* **1982**, *104*, 7519.
(18) Wacholtz, W. F.; Auerbach, R. A.; Schmehl, R. H. *Inorg. Chem.* **1986**, *25*, 227.
(19) (a) Becke, A. D. *J. Chem. Phys.* **1993**, *98*, 5648−5652. (b) Lee, C.; Yang, W.; Parr, R. G. *Phys. Rev. B* **1988**, *37*, 785−789.
(20) Zhao, Y.; Truhlar, D. G. *Theor. Chem. Acc.* **2006**, *120*, 215−241.
(21) Martin, J. M. L.; Sundermann, A. *J. Chem. Phys.* **2001**, *114*, 3408−3420.
(22) Marten, B.; Kim, K.; Cortis, C.; Friesner, R. A.; Murphy, R. B.; Ringnalda, M. N.; Sitkoff, D.; Honig, B. *J. Phys. Chem.* **1996**, *100*, 11775−11788.
(23) Tissandier, M. D.; Cowen, K. A.; Feng, W. Y.; Gundlach, E.; Cohen, M. H.; Earhart, A. D.; Coe, J. V. *J. Chem. Phys. A* **1998**, *102*, 7787−7794.
(24) Zong, R.; Wang, D.; Hammitt, R.; Thummel, R. P. *J. Org. Chem.* **2005**, *71*, 167−175.
(25) Suen, H. F.; Wilson, S. W.; Pomerantz, M.; Walsh, J. L. *Inorg. Chem.* **1989**, *28*, 786−791.
(26) Tong, L.; Duan, L.; Xu, Y.; Privalov, T.; Sun, L. *Angew. Chem., Int. Ed.* **2011**, *50*, 445−449.
(27) Umena, Y.; Kawakami, K.; Shen, J.-R.; Kamiya, N. *Nature* **2011**, *473*, 55−60.
(28) Kuznetsov, A. E.; Geletii, Y. V.; Hill, C. L.; Morokuma, K.; Musaev, D. G. *J. Am. Chem. Soc.* **2009**, *131*, 6844−6854.
(29) Besker, N.; Coletti, C.; Marrone, A.; Re, N. *J. Phys. Chem. B* **2008**, *112*, 3871−3875.
(30) White, H. S.; Becker, W. G.; Bard, A. J. *J. Phys. Chem.* **1984**, *88*, 1840.
(31) (a) Duan, L.; Xu, Y.; Zhang, P.; Wang, M.; Sun, L. *Inorg. Chem.* **2010**, *49*, 209−215. (b) Xu, Y.; Duan, L.; Tong, L.; Åkermark, B.; Sun, L. *Chem. Commun.* **2010**, *46*, 6506−6508.
(32) Geletii, Y. V.; Huang, Z.; Hou, Y.; Musaev, D. G.; Lian, T.; Hill, C. L. *J. Am. Chem. Soc.* **2009**, *131*, 7522−7523.